High order schemes for solving the time-dependent Schrödinger equation

D.A. Volobueva[a,b], *A.A. Gusev*[a,c,d], *O. Chuluunbaatar*[a,d,e], *V.L. Derbov*[f], *S.I. Vinitsky*[a,g]

[a] Joint Institute for Nuclear Research, Dubna, Russia
[b] Lomonosov Moscow State University Branch in Dubna, Dubna, Russia
[c] Dubna State University, Dubna, Russia
[d] Mongolian University of Science and Technology, Ulaanbaatar, Mongolia
[e] Institute of Mathematics and Digital Technology, Mongolian Academy of Sciences, Ulaanbaatar, Mongolia
[f] Saratov State University, Saratov, Russia
[g] Peoples' Friendship University of Russia named after Patrice Lumumba, Moscow, Russia

Implicit high-order operator-difference schemes for solving initial-boundary value problems (IBVPs) for the time-dependent Schrödinger equation (TSDE) are constructed. These multilayer schemes are based on the Magnus expansion of the evolution operator and Padé approximations. The solution is discretized with respect to the spatial variable using the finite element method with Hermite interpolation polynomials, ensuring the required smoothness of the solution. The convergence of the proposed schemes is demonstrated using benchmark IBVP calculations for the TSDE, which describes the evolution of several quantum systems.

INTRODUCTION

The time dependent Schrödinger equation (TDSE) is a basic mathematical model for describing the dynamics of a wide class of quantum systems [1]. Correct and efficient numerical solution of the initial boundary value problem (IBVP) for the TDSE requires the use of robust and highly accurate methods that preserve the fundamental physical properties of the system. An effective approach to constructing operator-difference schemes for solving TDSE based on operator differentiation technique and the Magnus expansion of the unitary evolution operator with the unitary Padé approximation [2,3] was constructed. Based on them some multilayer operator-difference schemes with spatial discretization by finite element method (FEM) are realized [4,5]. These schemes also have an accuracy of up to sixth order, provided that the commutator of the first and second derivatives of the Hamiltonian with respect to the time variable is zero. Note that with high-order discretization, the operator-difference scheme contains high-order derivatives, which requires high smoothness of the piecewise polynomial FEM functions.

The objective of this work is to construct and implement fourth- and six-order schemes for solving the one-dimensional TDSE based on the factorization of the unitary evolution operator with respect to the time variable with approximation by the high-order finite element method with Hermite interpolation polynomials (HIPs) [7] with respect to the spatial variable.

1. The problem statement

An IBVP for the TDSE is

$$\begin{aligned} &\imath\frac{\partial\psi(x,t)}{\partial t} = H(x,t)\psi(x,t), \quad H(t) = -\frac{1}{g_0(x)}\frac{d}{dx}g(x)\frac{d}{dx} + V(x,t), \\ &\psi(x,t_0) = \psi_0(x), \quad t \in [t_0,T], \quad x \in \Omega \subset \mathcal{R}. \end{aligned} \tag{1}$$

A square-integrable solution $\psi(x,t)$ from the Sobolev space $\mathcal{W}_2^2(\Omega)$ is subject to the Neumann (or Dirichlet) boundary conditions and the normalization condition:

$$\|\psi(x,t)\|^2 = \int_\Omega |\psi(x,t)|^2 dx = 1. \tag{2}$$

To solve the IBVP (1) on a time grid $t \in \{t_0, t_1, ..., t_k, t_{k+1}, ..., t_K = T\}$ in paper [4] the $2M$ order operator-difference scheme was formulated:

$$\begin{aligned} \hat{\psi}_k &= \psi(x,t_k), \\ \left(I + \frac{\tau\bar{\alpha}_\zeta^{(M)}}{2M}A_k^{(M)}\right)\hat{\psi}_{k+\zeta/M} &= \left(I + \frac{\tau\alpha_\zeta^{(M)}}{2M}A_k^{(M)}\right)\hat{\psi}_{k+(\zeta-1)/M}, \\ \psi(x,t_{k+1}) &= \hat{\psi}_{k+1}. \end{aligned} \tag{3}$$

Here I is the unit operator, coefficients $\alpha_\zeta^{(M)}$ at $\zeta = 1, \ldots, M$ are roots of the confluent hypergeometric function ${}_1F_1(-M, -2M, 2M\imath/\alpha)$.

The first three approximations of the exponential for the final effective Hamiltonians $A_k^{(M)}$ in the form $A_k^{(M)} = \hat{A}_k^{(M)} + \imath\breve{A}_k^{(M)}$

$$\begin{aligned} \hat{A}_k^{(1)} &= H, \\ \breve{A}_k^{(1)} &= 0, \\ \hat{A}_k^{(2)} &= \hat{A}_k^{(1)} + \frac{\tau^2}{24}\ddot{H}, \\ \breve{A}_k^{(2)} &= \breve{A}_k^{(1)} + \frac{\tau^2}{12}[H,\dot{H}], \\ \hat{A}_k^{(3)} &= \hat{A}_k^{(2)} + \frac{\tau^4}{1920}\dddot{H} - \frac{\tau^4}{720}[H,[H,\ddot{H}]] - \frac{\tau^4}{240}[\dot{H},[\dot{H},H]], \\ \breve{A}_k^{(3)} &= \breve{A}_k^{(2)} - \frac{\tau^4}{480}[\dddot{H},H] + \frac{\tau^4}{480}[\ddot{H},\dot{H}] + \frac{\tau^4}{720}[H,[H,[H,\dot{H}]]], \end{aligned}$$

where $H \equiv H(x,t_c)$, $\dot{H} \equiv \partial_t H(x,t)|_{t=t_c}, \ldots$

For the $H(x,t) = -\frac{1}{g_0(x)}\frac{d}{dx}g(x)\frac{d}{dx} + V(x,t)$ in the form (1) the operators $A_k^{(M)}$ have of the form calculated by substitution of hamiltonian (1) in definition of $A_k^{(M)}$ via commutators

$$\begin{aligned} A_k^{(M)} = -\frac{1}{g_0(x)}\frac{d}{dx}g^{(M)}\frac{d}{dx} + V^{(M)} - \frac{1}{g_0(x)}\left(Q^{(M)}\frac{d}{dx} - \frac{d}{dx}Q^{(M)}\right) \\ - \frac{1}{g_0(x)}\left(\frac{d^2}{dx^2}W^{(M)}\frac{d}{dx} - \frac{d}{dx}W^{(M)}\frac{d^2}{dx^2}\right), \end{aligned}$$

where

$$g^{(1)} = g^{(2)} = g(x), \quad g^{(3)} = g^{(2)} + \tau^4 \Big(g^{(3:22)} \ddot{V}''(x,t_c) + g^{(3:12)} \ddot{V}'(x,t_c) \Big)$$

$$V^{(1)} = V(x,t_c), \quad V^{(2)} = V^{(1)} + \frac{\tau^2}{24} \ddot{V}(x,t_c),$$

$$\begin{aligned} V^{(3)} = V^{(2)} + \tau^4 \Big(& V^{(3:04)} \dddot{V}(x,t_c) + V^{(3:12,10)} \ddot{V}'(x,t_c) V'(x,t_c) \\ & + V^{(3:11,11)} \dot{V}'(x,t_c)^2 + V^{(3:32)} \ddot{V}'''(x,t_c) + V^{(3:42)} \ddot{V}''''(x,t_c) \\ & + V^{(3:22)} \ddot{V}''(x,t_c) + V^{(3:12)} \ddot{V}'(x,t_c) \Big) \end{aligned}$$

$$Q^{(1)} = 0, \quad Q^{(2)} = Q^{(1)} + \frac{\imath\tau^2}{12} g(x) \dot{V}'(x,t_c),$$

$$\begin{aligned} Q^{(3)} = Q^{(2)} + \imath\tau^4 \Big(& Q^{(3:11)} \dot{V}'(x,t_c) \\ & + Q^{(3:21)} \dot{V}''(x,t_c) + Q^{(3:31)} \dot{V}'''(x,t_c) + Q^{(3:41)} \dot{V}''''(x,t_c) \\ & + Q^{(3:51)} \dot{V}'''''(x,t_c) + Q^{(3:13)} \dddot{V}'(x,t_c) + Q^{(3:11,10)} \dot{V}'(x,t_c) V'(x,t_c) \\ & + Q^{(3:20,11)} V''(x,t_c) \dot{V}'(x,t_c) + Q^{(3:10,21)} V'(x,t_c) \dot{V}''(x,t_c) \Big), \end{aligned}$$

$$W^{(1)} = W^{(2)} = 0$$

$$W^{(3)} = \imath\tau^4 \Big(W^{(3:11)} \dot{V}'(x,t_c) + W^{(3:21)} \dot{V}''(x,t_c) + W^{(3:31)} \dot{V}'''(x,t_c) \Big)$$

where dot $\dot{}$ and prime $'$ at V means its derivatives by t and x, respectively.

The coefficiens $g^{(3:**)}$, $V^{(3:**)}$, $V^{(3:**,**)}$, $Q^{(3:**)}$, $Q^{(3:**,**)}$ and $W^{(3:**)}$ are the calculated functions of $g_0(x)$ and $g(x)$ given in Appendix.

Thus, an implicit numerical scheme of order $2M$ is obtained. It is stable, since it preserves the norm of the difference solution.

Note that for $M = 1$, $\alpha_1^{(1)} = -\imath$, and the scheme (3), known as the Crank-Nicolson scheme [6], is second-order($2M = 2$) in τ_k.

For $M = 2$, $\alpha_\zeta^{(2)} = (-1)^{\zeta+1}/\sqrt{3} - \imath$, and the scheme (3) is fourth-order ($2M = 4$) in τ_k.

For $M = 3$: $\alpha_1^{(3)}$=0.8147995542489228$-\imath$0.8540567306516635,
$\alpha_2^{(3)}$=$-\imath$1.2918865386966731 $\alpha_3^{(3)}$=$-$0.8147995542489228$-\imath$0.8540567306516635, and the scheme (3) is six-order ($2M = 6$) in τ_k.

To analyze the convergence on a sequence of three doubly-condenced time grids, we define the auxiliary time dependent discrepancy functions

$$Er^2(t,j) = \int_{x_{\min}}^{x_{\max}} |\psi(x,t_k) - \psi^{\tau_j}(x,t_k)|^2 dx, \quad j = 1,2,3, \tag{4}$$

and the Runge coefficient

$$\beta(t) = \log_2 \left| \frac{Er(t,1) - Er(t,2)}{Er(t,2) - Er(t,3)} \right|, \tag{5}$$

where $\psi^{\tau_j}(x,t)$ are the numerical solutions with the time step $\tau_j = \tau/2^{j-1}$. For the function $\psi(x,t)$ one can use the numerical solution with the time step $\tau_4 = \tau/8$. Hence, we obtain the numerical estimates for the convergence order of the numerical scheme, that strongly correspond to theoretical ones $\beta(t) \equiv \beta_M(t) \approx 2M$. The solution is discretized with respect to the spatial variable using the finite element method with Hermite interpolation polynomials (HIPs) [7], ensuring the required smoothness of the solution.

Example 1: 1D harmonic oscillator in the electric field

A software implementation of the described computational scheme was developed for the 1D harmonic oscillator in the electric field. The IBVP

$$H(x,t) = -\frac{d^2}{dx^2} + x^2 + fx\sin(\omega t), \quad \psi(x,t_0) = \pi^{-1/4}\exp(-x^2/2). \tag{6}$$

has the analytical solution

$$\psi_{ext}(x,t) = \pi^{-1/4}\exp(-x^2/2 - xB(t) - C(t)), \tag{7}$$

where $B(t)$ and $C(t)$ are coefficients obtained by substitution (7) to (9) (see [1]).

Benchmark calculations. The calculations were performed on spatial finite element mesh $x = \{-8(0.2)8\}$ with fifth-order HIPs and time grids $t \in \{0(\tau)20\}$ at $\tau = 0.2, 0.1, 0.05, 0.025$. The discrepancy functions $Er(t,j)$ and the Runge coefficient $\beta(t)$ are presented in Figure 1. One can see that Runge coefficient closes to its theoretical estimation Ru $\approx 2M$ that is approved the $2M$ order of the developed scheme.

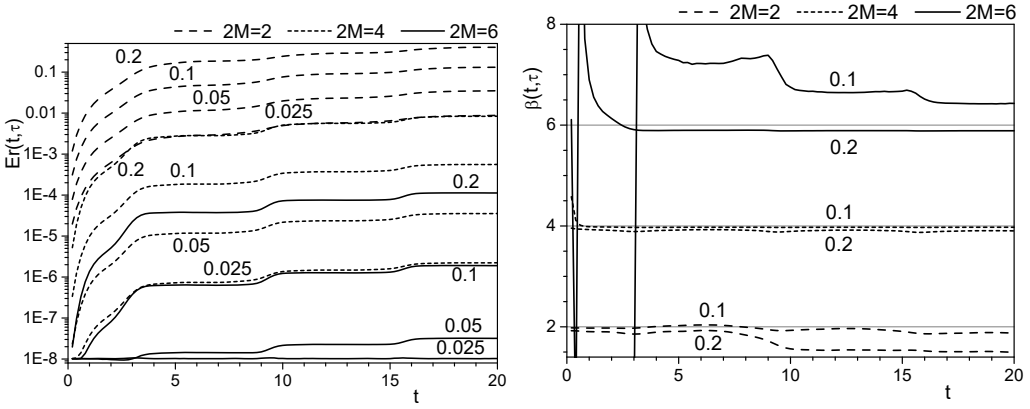

Figure 1. The auxiliary time dependent discrepancy functions $Er(t,j)$ and the Runge coefficient $\beta(t)$ in depends on t

Example 2. An atom in the field of a short laser π-pulse

Initial-boundary value problem for a time-dependent Schrödinger equation of a model of one-dimensional atom (with potential $V(x) = \cosh^{-2} x$ in an external field $q(x,t)$ on a time interval $t \in [t_0, T]$) has the form

$$\imath \frac{\partial}{\partial t}\psi(x,\, t) = (-\frac{1}{2}\frac{\partial^2}{\partial x^2} + V(x) + q(x,t))\psi(x,\, t),\; q(x,t) = f(t)x \quad (8)$$
$$\psi(x,t_0) = \psi_0(x), \quad \psi(-\infty,t) = \psi(\infty,t) = 0, \quad ||\psi(x,t)|| = 1$$

in the field $q(x,t) = f(t)x$ of a short laser π pulse:

$$f(t) = \{f_0 \cos^2(\frac{\pi t}{2t_0}), -t_0 < t < t_0; 0, |t| \geq t_0, \}$$

at $f_0 = t_0 = 1$. The real and imaginary parts of solution $\psi^\tau(x,t_k)$ at $t = 0$ and $t = 9$ are presented in Figure 2.

Benchmark calculations. The calculations were performed on spatial finite element mesh $x = \{-80(1)40\}$ with fifth-order HIPs and time grids $t \in \{-1(\tau)9\}$ at $\tau = 0.2, 0.1, 0.05, 0.025$. The discrepancy functions $Er(t,j)$ and the Runge coefficient $\beta(t)$ are presented in Figure 3. One can see that Runge coefficient closes to its theoretical estimation $\mathrm{Ru} \approx 2M$ that is approved the $2M$ order of the developed scheme.

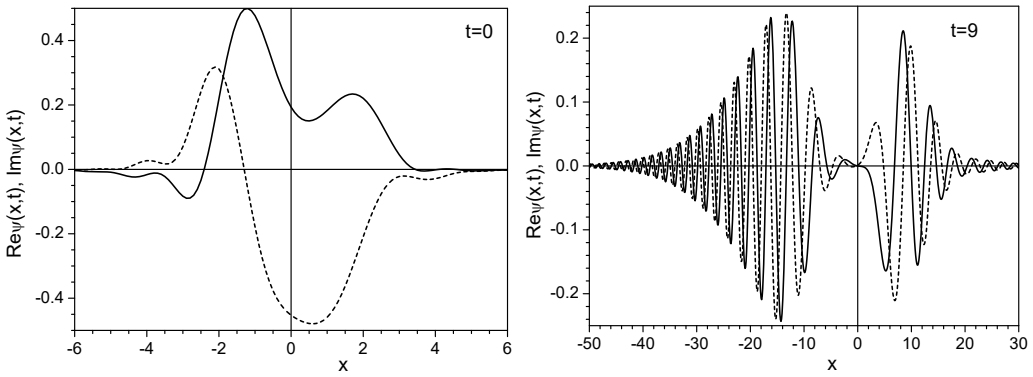

Figure 2. The real (solid curves) and imaginary (dashed curves) parts of solution $\psi^\tau(x,t_k)$ at $t = 0$ and $t = 9$.

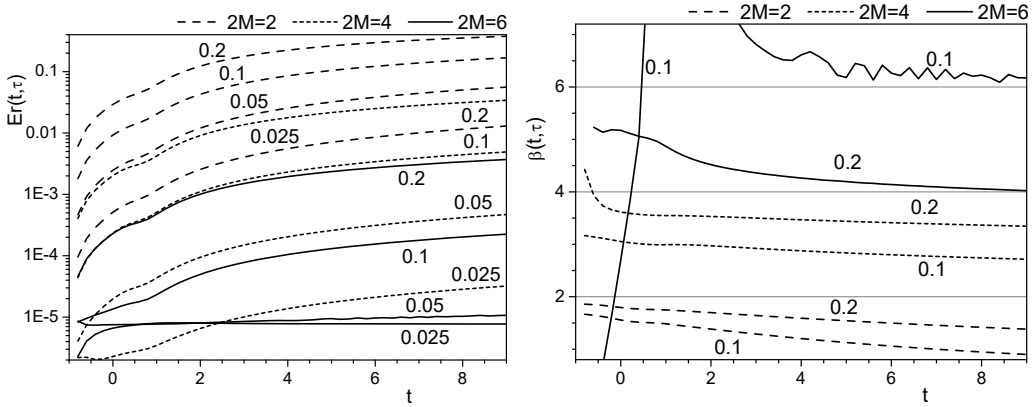

Figure 3. The auxiliary time dependent discrepancy functions $Er(t,j)$ and the Runge coefficient $\beta(t)$ in depends on t

Example 3: two-center problem with Pöschl-Teller potentials

As next example we solve the two-center problem with Pöschl-Teller potentials similar to an ionization problem. We choose a special case of a resting well, $A_0 < 0$, and a barrier, $A_1 > 0$ (or a well $A_1 < 0$), that moved with velocity v with respect to the resting well:

$$H(x,t) = -\frac{1}{2}\frac{d^2}{dx^2} + \frac{A_0}{\cosh^2 x} + \frac{A_1}{\cosh^2(x-vt)}, \quad \psi(x,t_0) = \frac{1}{\sqrt{\pi}\cosh^2 x}. \quad (9)$$

The evolution of the wave packet in the time-interval $t \in [t_0 = -20, T = 20]$, induced by the moving barrier ($A_1 = 15/8$) with velocity $v = 1/2$, with respect to the resting well ($A_0 = -15/8$) supporting two bound states first of them is chosen as the initial state.

Benchmark calculations. The calculations were performed on spatial finite element mesh $x = \{-40(1)60\}$ with fifth-order HIPs and time grids $t \in \{-6(\tau)18\}$ at $\tau = 1., 0.5, 0.25, 0.125$. The discrepancy functions $Er(t,j)$ and the Runge coefficient $\beta(t)$ are presented in Figure 4. One can see that Runge coefficient closes to its theoretical estimation Ru $\approx 2M$ are different from $2M$ because in this case the rounding error makes a large contribution to the error.

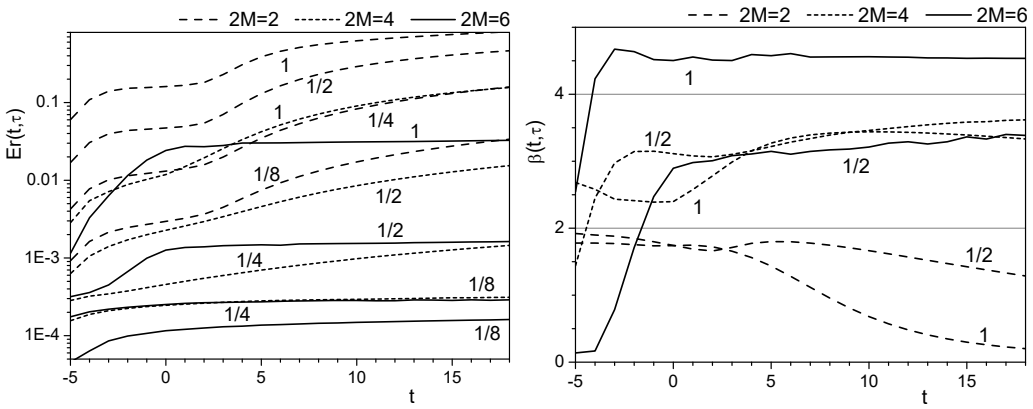

Figure 4. The auxiliary time dependent discrepancy functions $Er(t,j)$ and the Runge coefficient $\beta(t)$ in depends on t

The wave function and the distribution of ionization probability $p_E(t)$ vs the time t are shown in Figure 5. Dependence of eigenenergies $E_n < 0$ of the instant Hamiltonian on time parameter t is shown in Figure 6a. One can see that in a vicinity of time value $t = 0$ the Hamiltonian has only one eigenvalue $E_1 < 0$ and at time $t = 0$ it has only continuous spectrum. After that the effective potential becomes again nonzero and processes of captures to the exited and ground states may occur which is shown by evolution of probabilities $p_E(t)$ and $p_c(t)$ in Figure 6b. In Figure 5 it is shown that at $t \geq 1$ the maxima of energy distribution $p_{E\sim 1} \sim 0.5$ correspond to the forward and backward ionization waves with similar frequencies moved to left and right. The maxima of $p_c(t)$ at $t \sim 4$ on Figure 6 correspond to the maxima of $p_{E\sim 0.01} \sim 1$ at frame $t = 4$ on Figure 5b and coincide with ionization and capture processes.

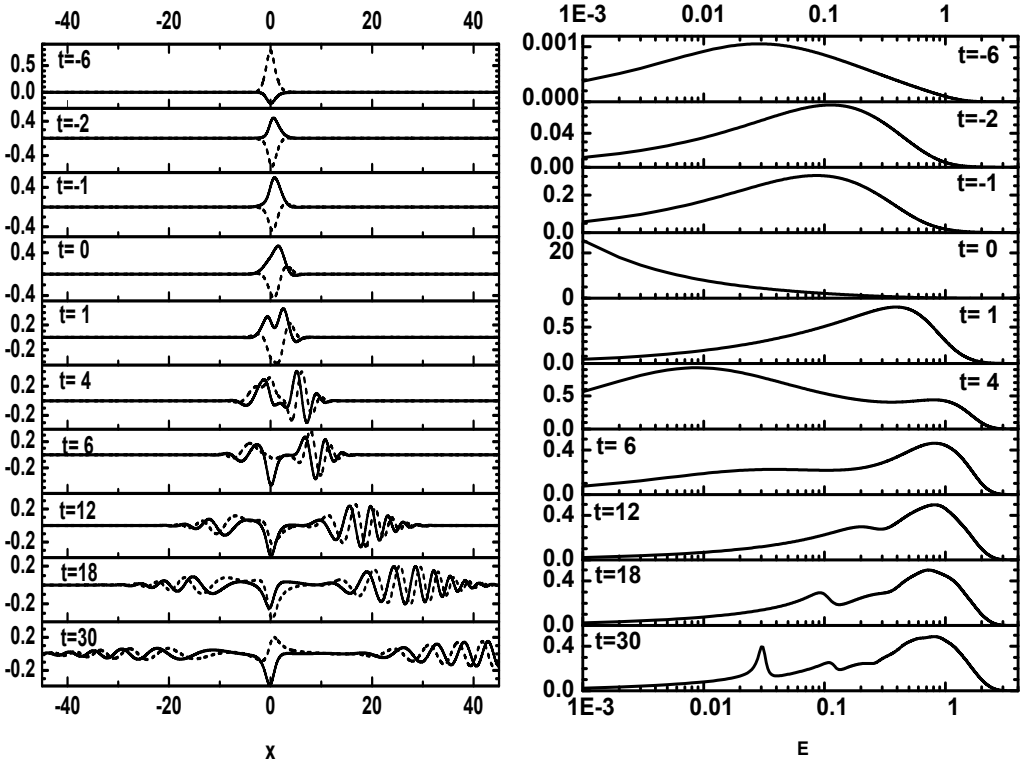

Figure 5. Real (solid line), image (dashed line) parts of the wave function and the distribution of ionization probability $p_E(t)$ vs the time t for fixed value of velocity $v = 1/2$ and initial position of the moving barrier $x_0(t_0) = vt_0 = -15$, $t_0 = -30$.

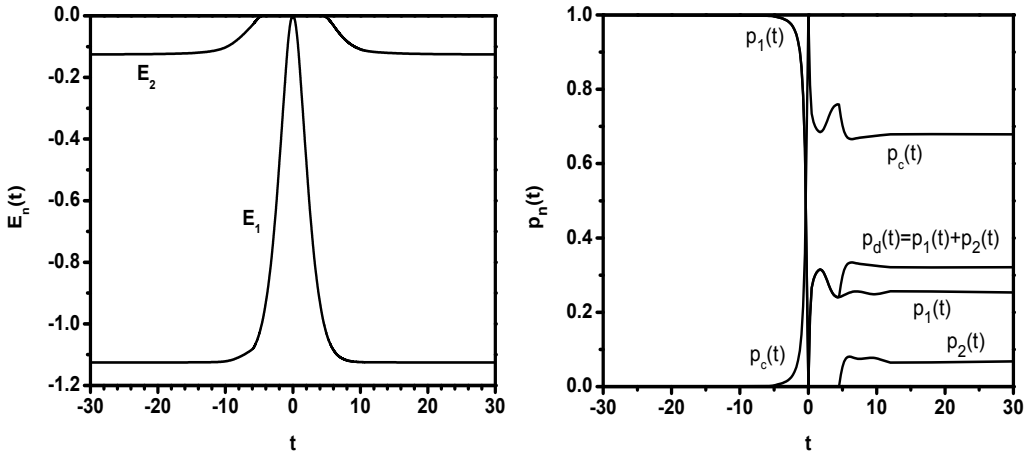

Figure 6. Eigenenergies $E_n(t) = E_n(R(t))$ or potential curves of the instant Hamiltonian in dependence of the time as a parameter t or $R(t)$ – distance between target and projectile. The bound state probabilities $p_1(t)$, $p_2(t)$ and the ionization probability $p_c(t)$ vs the time t. Here $v = 1/2$, $x_0(t_0) = vt_0 = -15$, $t_0 = -30$.

The wave function and the distribution of ionization probability $p_E(t)$ for some values of velocity are shown in Figure 7. As it is seen from Figure 7 with increasing v the forward ionization waves dominate and their energy

increase. With increasing velocity the probability densities of the excited states at large velocity tend to zero (see Figure 8).

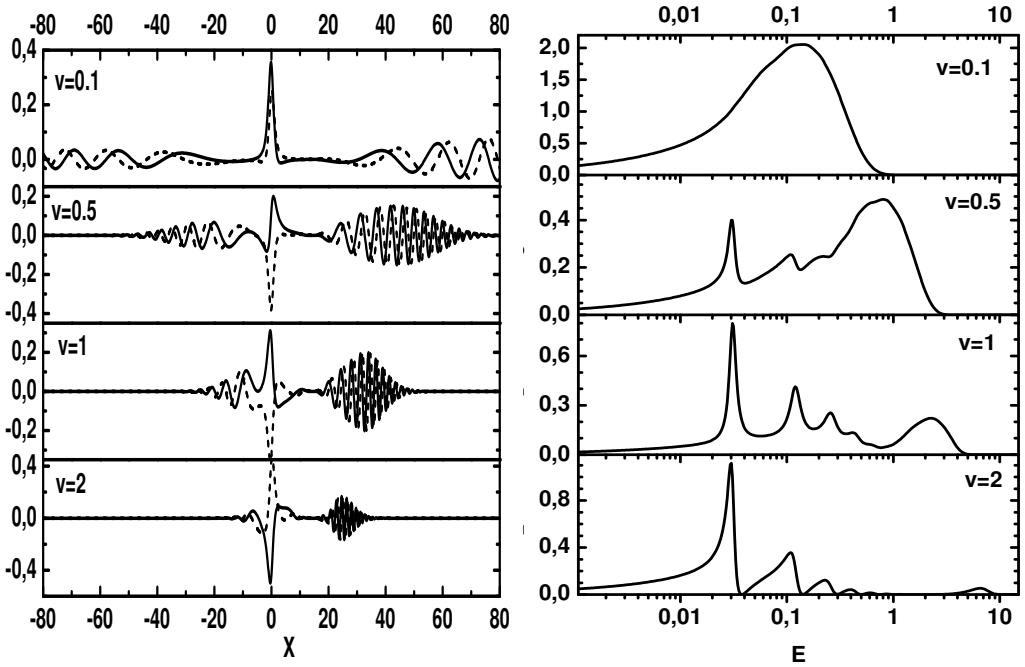

Figure 7. a) Real (solid line), image (dashed line) parts of the wave function and b) the distribution of ionization probability $p_E(T)$ by energy E for fixed values of velocity $v = 0.1, 0.5,\ 1,\ 2$.

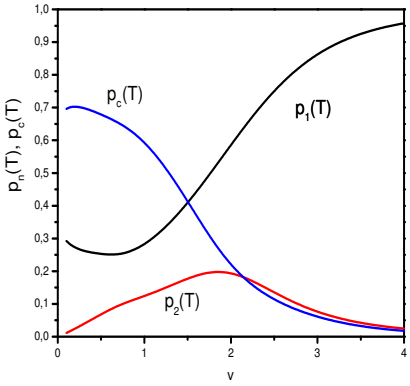

Figure 8. The probabilities $p_1(T)$, $p_2(T)$ of ground and first excited states, and ionization probability $p_c(T)$ vs velocity v for time $T = 15/v$ and initial time $t_0 = -15/v$ when the position of the center of barrier is equal $x_0(T) = 15$ and $x_0(t_0) = -15$, correspondingly.

CONCLUSIONS

In this work, a fourth order scheme for solution of an IBVP for the TDSE was constructed and implemented in Wolfram Mathematica. Numerical experiments confirmed known theoretical estimates of the fourth order scheme. Based on this the schemes with automatical selection of the optimal step by spatial and time variables will be constructed that is important for the correct modeling of nuclear reactions.

A. The coefficiens $g^{(3:**)}$, $V^{(3:**)}$, $V^{(3:**,**)}$, $Q^{(3:**)}$, $Q^{(3:**,**)}$ and $W^{(3:**)}$

$$
\begin{aligned}
g^{(3:22)} &= \frac{g(x)^2}{180g_0(x)}, \\
g^{(3:12)} &= \frac{g(x)g'(x)}{360g_0(x)} - \frac{g_0'(x)g(x)^2}{360g_0(x)^2}, \\
V^{(3:04)} &= \frac{g_0(x)}{1920}, \\
V^{(3:12,10)} &= -\frac{g(x)}{360}, \\
V^{(3:11,11)} &= \frac{g(x)}{120}, \\
V^{(3:32)} &= \frac{g_0'(x)g(x)^2}{360g_0(x)^2} - \frac{g(x)g'(x)}{180g_0(x)}, \\
V^{(3:42)} &= -\frac{g(x)^2}{720g_0(x)}, \\
V^{(3:22)} &= -\frac{g_0'(x)^2g(x)^2}{360g_0(x)^3} + \frac{g_0''(x)g(x)^2}{720g_0(x)^2} + \frac{g_0'(x)g'(x)g(x)}{144g_0(x)^2} - \frac{g''(x)g(x)}{240g_0(x)} - \frac{g'(x)^2}{360g_0(x)}, \\
V^{(3:12)} &= -\frac{g_0'(x)^2g'(x)g(x)}{360g_0(x)^3} + \frac{g_0''(x)g'(x)g(x)}{720g_0(x)^2} + \frac{g_0'(x)g''(x)g(x)}{360g_0(x)^2} \\
&\quad -\frac{g'''(x)g(x)}{720g_0(x)} + \frac{g_0'(x)g'(x)^2}{720g_0(x)^2} - \frac{g''(x)g'(x)}{720g_0(x)}, \\
\\
Q^{(3:51)} &= \frac{g(x)^3}{720g_0(x)^2}, \\
Q^{(3:13)} &= \frac{g(x)}{480}, \\
Q^{(3:20,11)} &= \frac{g(x)^2}{360g_0(x)} \\
Q^{(3:41)} &= \frac{g'(x)g(x)^2}{120g_0(x)^2} - \frac{g_0'(x)g(x)^3}{180g_0(x)^3} \\
Q^{(3:10,21)} &= \frac{g(x)^2}{120g_0(x)}, \\
Q^{(3:11)} &= \frac{g(x)^2g''''(x)}{720g_0(x)^2} + \frac{g(x)g''(x)^2}{720g_0(x)^2} + \frac{g_0'(x)^2g''(x)g(x)^2}{90g_0(x)^4} - \frac{g_0''(x)g''(x)g(x)^2}{240g_0(x)^3} \\
&\quad + \frac{g_0'(x)^2g'(x)^2g(x)}{144g_0(x)^4} - \frac{g_0''(x)g'(x)^2g(x)}{360g_0(x)^3} - \frac{g_0'(x)^3g'(x)g(x)^2}{90g_0(x)^5} \\
&\quad + \frac{7g_0'(x)g_0''(x)g'(x)g(x)^2}{720g_0(x)^4} - \frac{g_0'''(x)g'(x)g(x)^2}{720g_0(x)^3} - \frac{g_0'(x)g(x)^2g'''(x)}{180g_0(x)^3} \\
&\quad + \frac{g'(x)g(x)g'''(x)}{360g_0(x)^2} - \frac{g_0'(x)g(x)g'(x)g''(x)}{120g_0(x)^3},
\end{aligned}
$$

$$
\begin{aligned}
Q^{(3:31)} &= \frac{g_0'(x)^2 g(x)^3}{90 g_0(x)^4} - \frac{g_0''(x) g(x)^3}{240 g_0(x)^3} + \frac{7 g(x)^2 g''(x)}{720 g_0(x)^2} + \frac{g(x) g'(x)^2}{120 g_0(x)^2} - \frac{17 g_0'(x) g(x)^2 g'(x)}{720 g_0(x)^3}, \\
Q^{(3:21)} &= -\frac{g_0'(x)^3 g(x)^3}{90 g_0(x)^5} + \frac{7 g_0'(x) g_0''(x) g(x)^3}{720 g_0(x)^4} - \frac{g_0'''(x) g(x)^3}{720 g_0(x)^3} \\
&\quad - \frac{13 g_0'(x) g(x)^2 g''(x)}{720 g_0(x)^3} - \frac{g_0'(x) g(x) g'(x)^2}{72 g_0(x)^3} + \frac{7 g_0'(x)^2 g'(x) g(x)^2}{240 g_0(x)^4} \\
&\quad - \frac{g_0''(x) g'(x) g(x)^2}{90 g_0(x)^3} + \frac{g(x)^2 g'''(x)}{180 g_0(x)^2} + \frac{g'(x) g(x) g''(x)}{90 g_0(x)^2}, \\
Q^{(3:11,10)} &= \frac{g'(x) g(x)}{180 g_0(x)} - \frac{g_0'(x) g(x)^2}{180 g_0(x)^2},
\end{aligned}
$$

$$
\begin{aligned}
W^{(3:31)} &= \frac{g(x)^3}{180 g_0(x)^2}, \\
W^{(3:21)} &= -\frac{g_0'(x) g(x)^3}{120 g_0(x)^3} + \frac{g(x)^2 g'(x)}{120 g_0(x)^2}, \\
W^{(3:11)} &= \frac{g_0'(x)^2 g(x)^3}{180 g_0(x)^4} - \frac{g_0''(x) g(x)^3}{360 g_0(x)^3} - \frac{g_0'(x) g(x)^2 g'(x)}{180 g_0(x)^3} + \frac{g(x)^2 g''(x)}{360 g_0(x)^2}.
\end{aligned}
$$

REFERENCES

1. *Butkovskiy A.G., Samoilenko Yu.I.* Control of Quantum-Mechanical Processes and Systems. — Dordrecht Hardbound: Kluwer, 1990.

2. *Magnus W.* On the exponential solution of differential equations for a linear operator // Commun. Pure Appl. Math. — 1954. — V. 7. — P. 649–673. — https://doi.org/10.1063/1.1705306.

3. *Wilcox R.M.* Exponential Operators and Parameter Differentiation in Quantum Physics // J. Math. Phys. — 1967. — V. 8. — P. 962–982. — https://doi.org/10.1063/1.1705306.

4. *Puzynin I.V., Selin A. V. and. Vinitsky S.I.* Magnus-factorized method for numerical solving the time-dependent Schrödinger equation // Comput. Phys. Commun. — 2000. — V. 126. — P. 158–161. — https://doi.org/10.1016/S0010-4655(99)00225-8.

5. *Chuluunbaatar O., Derbov V.L., Galtbayar A., Gusev A.A., Kaschiev M.S., Vinitsky S.I., Zhanlav T.* Explicit Magnus expansions for time-dependent Schrödinger equation // J. Phys. A. — 2008. — V. 41. — P. 295203. — https://iopscience.iop.org/article/10.1088/1751-8113/41/29/295203.

6. *Crank J., Nicolson P.* A practical method for numerical evaluation of solutions of partial differential equations of the heat-conduction type. // Proc. Camb. Phil. Soc. — 1947. — V. 43. — P. 50–67. — https://doi.org/10.1007/BF02127704.

7. *Gusev A., Chuluunbaatar O., Vinitsky S., Derbov V., A. G., Hai L., Rostovtsev V.* Symbolic-numerical solution of boundary-value problems with self-adjoint second-order differential equation using the finite element method with interpolation Hermite polynomials // Lecture Notes Computer Sci. — 2014. — V. 8660. — P. 138–154. — https://doi.org/10.1007/978-3-319-10515-4_11.